

Sensing Safety Analysis for Vehicular Networks with Integrated Sensing and Communication (ISAC)

Tingyu Shui¹, Walid Saad¹, and Mingzhe Chen²

¹Bradley Department of Electrical and Computer Engineering, Virginia Tech, Alexandria, VA, 22305, USA.

²Department of Electrical and Computer Engineering and Frost Institute for Data Science and Computing, University of Miami, Coral Gables, FL, 33146, USA.

Emails: {tygrady, walids}@vt.edu, mingzhe.chen@miami.edu

Abstract—Integrated sensing and communication (ISAC) emerged as a key feature of next-generation 6G wireless systems, allowing them to achieve high data rates and sensing accuracy. While prior research has primarily focused on addressing communication safety in ISAC systems, the equally critical issue of sensing safety remains largely ignored. In this paper, a novel threat to the sensing safety of ISAC vehicle networks is studied, whereby a malicious reconfigurable intelligent surface (RIS) is deployed to compromise the sensing functionality of a roadside unit (RSU). Specifically, a malicious attacker dynamically adjusts the phase shifts of an RIS to spoof the sensing outcomes of a vehicular user (VU)’s echo delay, Doppler shift, and angle-of-departure (AoD). To achieve spoofing on Doppler shift estimation, a time-varying phase shift design on the RIS is proposed. Furthermore, the feasible spoofing frequency set with respect to the Doppler shift is analytical derived. Analytical results also demonstrate that the maximum likelihood estimator (MLE) of the AoD can be significantly misled under spoofed Doppler shift estimation. Simulation results validate our theoretical findings, showing that the RIS can induce a spoofed velocity estimation from 0.1 m/s to 14.9 m/s for a VU with velocity of 10 m/s, and can cause an AoD estimation error of up to 65° with only a 5° beam misalignment.

Index Terms—ISAC, Sensing safety, Vehicular network, RIS, Spoofing.

I. INTRODUCTION

Integrated sensing and communication (ISAC) is a promising 6G technology for vehicular applications that require both high-quality communication and high-accuracy sensing such as connected autonomous vehicle (CAV) and cooperative perception (CP). ISAC allows a wireless base station (BS) to simultaneously provide communication and sensing functions through the co-design of the hardware architecture, transmitted waveforms, and signal processing algorithms. However, the joint design of sensing and communications coupled with the broadcast nature of wireless transmission in ISAC networks will introduce critical security and safety problems [1].

Aligned with the dual functionalities, ISAC networks’ security concerns should be addressed from two distinct perspectives: *communication safety* and *sensing safety*. A number of recent works have studied the communication safety issue, in which ISAC networks are designed to be resilient to eavesdropping attacks [2]–[5]. Specifically, these studies consider eavesdroppers that act as sensing targets to intercept ISAC signals. However, the issue of sensing safety received far less attention. Unlike information leakage, which is the primary concern in communication safety, sensing safety

attacks focus on adversarially manipulating and spoofing the sensing outcomes of an ISAC system [6]. Such attacks on sensing safety may lead to severe consequences. For example, in an ISAC-enabled vehicular application, a pedestrian may become undetectable to a CAV under a spoofing attack that targets the sensing outcome.

There are only a few preliminary works that looked at this sensing safety problems and its challenges [7]–[10]. Specifically, these works, from a defender’s perspective, aim to conceal targets from being detected by unauthorized ISAC stations. Inspired by electronic countermeasure (ECM) techniques, the authors in [7]–[9] leverage a novel reconfigurable intelligent surface (RIS)-aided framework where the sensing echos received at the unauthorized ISAC station are suppressed while those received at the authorized ISAC station are enhanced. Particularly, the RIS, acting as an intelligent ECM, is mounted on the target for directional radar stealth. In [10], the RIS is further exploited to simultaneously conceal the target and spoof the unauthorized ISAC station. By redirecting the detection signal to clutter, the RIS generates a deceptive angle-of-arrival (AoA) sensing outcome on the unauthorized ISAC stations. However, the works in [7]–[10], which leverage RIS to enhance the sensing safety of ISAC networks, also raise a critical question: *Can a malicious RIS be exploited to compromise the sensing safety of ISAC networks instead? If so, how would this malicious RIS be designed, and what impact would it have on the sensing outcomes?*

The main contribution of this paper is a novel RIS-aided spoofing technique that can be shown to compromise the sensing safety of an ISAC vehicular network. In our considered system, an attacker deploys a malicious RIS in the coverage of a roadside unit (RSU). Different from the directional radar stealth methods proposed in [7]–[10], the malicious RIS is fixed in location rather than being mounted on the sensing target, such as vehicular users (VUs), which makes the spoofing much more practical. We particularly propose a time-varying phase shifts design on the RIS to spoof the RSU’s estimation on the VU’s echo delay, Doppler shift, and angle-of-departure (AoD). We then derive the closed-form expressions of the phase shifts design and the feasible spoofing frequencies set with respect to the Doppler shift. Moreover, we analytically show that, the maximum likelihood estimator (MLE) of the AoD will also be jeopardized under the proposed RIS spoofing. To our best knowledge, *this is*

the first work that designs RIS to compromise the sensing safety of ISAC network and analyzes its impact on the resulted sensing outcome. Simulation results demonstrate that, given a 10 m/s true velocity for the VU, the RIS can cause a spoofed velocity estimation from 0.1 m/s to 14.9 m/s and a spoofed AoD estimation of deviation up to 65° , even with a beam misalignment of only 5° for the RSU.

The rest of the paper is organized as follows. The system model is presented in Section II. The design of RIS spoofing and the analysis of its impact on sensing safety are performed in Section III. Section IV presents the simulation results and Section V concludes the paper.

II. SYSTEM MODEL

Consider an ISAC system supported by a full-duplex millimeter wave (mmWave) RSU. The RSU is equipped with a uniform linear array (ULA) of N_t transmit antennas and N_r receive antennas to provide sensing and downlink communications to a single-antenna VU. By estimating the VU's kinetic states from echo signals, the RSU can support critical applications such as beam tracking and CAV trajectory planning. A two-dimensional Cartesian coordinate system is used with the RSU located at its origin. The goal of the RSU is to estimate the coordinates (x_V, y_V) and velocity v of the VU. However, a malicious RIS is deployed to compromise the RSU's sensing functionality by manipulating the echo signals, as shown in Fig. 1. Following a standard convention in the literature [11], we focus on the case in which the VU moves along a straight road parallel to the RSU's ULA¹.

A. Signal Model

Let $s(t) \in \mathbb{C}$ be the RSU's transmitted ISAC symbol with unit power, i.e., $s(t)s^*(t) = 1$. Given the precoding vector $\mathbf{w} \in \mathbb{C}^{N_t \times 1}$ at the RSU, the echo signal reflected by the VU can be modeled as follows:

$$\mathbf{y}_{E,V}(t) = \sqrt{P}\gamma_B\beta_V e^{j2\pi\mu_V t} \mathbf{b}_B(\theta_V) \mathbf{a}_B^H(\theta_V) \mathbf{w}s(t - \tau_V), \quad (1)$$

where P is the transmit power of the RSU, $\gamma_B = \sqrt{N_t N_r}$ is the array gain factor, and $\beta_V = \sqrt{\frac{\lambda^2 \kappa_V}{64\pi^3 d_V^4}} e^{\frac{j4\pi d_V}{\lambda}}$ combines the complex path gain of the RSU-VU-RSU link and the radar cross section (RCS) κ_V of the VU. The distance between the RSU and the VU is d_V and the carrier wavelength is λ . Meanwhile, the Doppler shift μ_V , AoD θ_V , and double-path echo delay τ_V of the VU are included in (1), where $\mathbf{a}_B(\theta)$ and $\mathbf{b}_B(\theta)$ are the steering vector of the transmitting and receiving antennas, respectively, at the RSU. By assuming a half-wavelength antenna space, $\mathbf{a}_B(\theta)$ and $\mathbf{b}_B(\theta)$ will be given by:

$$\mathbf{a}_B(\theta) = \frac{1}{\sqrt{N_t}} \left[1, e^{-j\pi \cos \theta}, \dots, e^{-j\pi(N_t-1) \cos \theta} \right]^T, \quad (2)$$

$$\mathbf{b}_B(\theta) = \frac{1}{\sqrt{N_r}} \left[1, e^{-j\pi \cos \theta}, \dots, e^{-j\pi(N_r-1) \cos \theta} \right]^T. \quad (3)$$

¹The extension to a non-parallel case is straightforward by rotating the coordinate system.

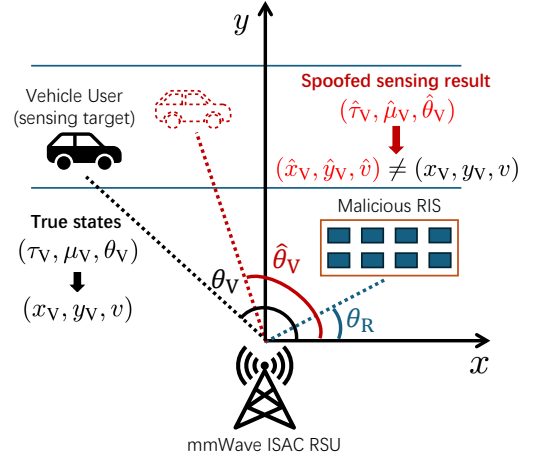


Fig. 1. System model of the considered ISAC network under the spoofing of a malicious RIS.

The sensing process on the RSU should estimate (x_V, y_V) and v of the VU, which can be derived from τ_V , μ_V , and θ_V . However, in the presence of the malicious RIS, the echo received by the RSU is a composition of the legitimate echo reflected by the VU and the spoofing echo adversarially reflected by the RIS. Assume that the reflecting elements of the RIS are formed as a ULA of M elements, the spoofing echo from the RIS can be similarly given by:

$$\mathbf{y}_{E,R}(t) = \sqrt{P}\gamma_B\beta_R \mathbf{b}_B(\theta_R) \mathbf{a}_R^H(\theta_B) \text{diag}[\phi(t)] \times \mathbf{b}_R(\theta_B) \mathbf{a}_B^H(\theta_R) \mathbf{w}s(t - \tau_R), \quad (4)$$

where $\beta_R = \sqrt{\frac{\lambda^2 \kappa_R}{64\pi^3 d_R^4}} e^{\frac{j4\pi d_R}{\lambda}}$ combines the complex path gain of the RSU-RIS-RSU link and the RCS κ_R of the RIS. According to [12], we have $\kappa_R = \frac{4\pi\eta S^2}{\lambda^2}$ with an RIS's reflection efficiency η , area S , and operating wavelength λ . Similarly, $\mathbf{b}_R(\cdot)$ and $\mathbf{a}_R(\cdot)$, θ_B , and τ_R are the steering vectors, AoA (and also AoD), and echo delay of the RIS. The phase shifts at the RIS are given by $\phi(t) = [e^{j\phi_1(t)}, e^{j\phi_2(t)}, \dots, e^{j\phi_M(t)}]$ and unit reflection amplitudes are assumed for simplicity. Note that $\phi(t)$ must be time-varying to spoof the sensing process, as we will explain in Section III. Thus, the composite echo received by the RSU can be given by:

$$\mathbf{y}_E(t) = \mathbf{y}_{E,R}(t) + \mathbf{y}_{E,V}(t) + \mathbf{z}_E(t), \quad (5)$$

where $\mathbf{z}_E(t) \sim \mathcal{CN}(0, \sigma^2 \mathbf{I}_M)$ is the additive white Gaussian noise (AWGN) at the RSU's receiving antennas.

B. Sensing Spoofing by Malicious RIS

We focus on the sensing process of a short interval T , defined as an epoch, during which (x_V, y_V) and v are assumed to be constant [13]. Within an arbitrary epoch, the RSU first determines μ_V and θ_V through a standard matched-filtering technique [11], after which the received signal in (5) is compensated in both time and frequency domain for further estimating θ_V . In particular, the matched-filtering output of $\mathbf{y}_E(t)$ is defined as follows:

$$C(\tau, \mu) \triangleq \left| \int_0^T \mathbf{y}_E(t) s^*(t - \tau) e^{-j2\pi\mu t} dt \right|^2. \quad (6)$$

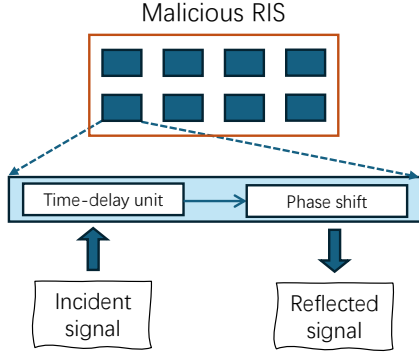


Fig. 2. The architecture of the adjustable-delay RIS.

Thus, the estimated echo delay and Doppler shift can be given by $(\hat{\tau}_V, \hat{\mu}_V) = \arg \max_{\tau, \mu} C(\tau, \mu)$. Moreover, we consider the MLE of θ_V , which can be given by:

$$\hat{\theta}_V = \arg \max_{\theta_V} p(\hat{\mathbf{y}}_E | \theta_V). \quad (7)$$

In (7), $\hat{\mathbf{y}}_E = \int_0^T \mathbf{y}_E(t) s^*(t - \hat{\tau}_V) e^{-j2\pi\hat{\mu}_V t} dt$ represents the echo compensated by $\hat{\tau}_V$ and $\hat{\mu}_V$.

The goal of the malicious RIS is to hinder the RSU from obtaining accurate $\hat{\tau}_V$, $\hat{\mu}_V$, and $\hat{\theta}_V$. In other words, the spoofing echo $\mathbf{y}_{E,R}(t)$ given in (4) is expected to cause a deviation in the peak position of $C(\tau, \mu)$ and further distort the accuracy of $\hat{\theta}_V$. In typical ISAC system of large bandwidth, the delay resolution of $C(\tau, \mu)$ is sufficiently high to resolve the two echoes given in (1) and (4). Thus, the spoofed echo can be mitigated if the echo delay difference satisfies $|\tau_V - \tau_R| \geq \tau_0$, where τ_0 is the effective main-lobe width of $C(\tau, \mu)$ in the time domain. To successfully conduct the echo spoofing, an adjustable-delay RIS [14] is implemented in our system, as shown in Fig. 2. Here, a time-delay unit is cascaded before the RIS's phase shifter such that it is able to store and retrieve the impinging signals with a designed delay Δt_R . As a result, the echo delay in (4) will be: $\tau_R = \Delta t_R + 2\frac{d_R}{c}$.

Remark 1. The reason for incorporating the adjustable-delay RIS is to ensure that $|\tau_V - \tau_R| < \tau_0$. Thus, $\hat{\tau}_V$ is not spoofed. Moreover, hereinafter, we focus on the case $|\tau_V - \tau_R| = 0$. As a result, a necessary condition for the RIS echo spoofing is $0 \leq \Delta t_R = 2\frac{d_V - d_R}{c} \leq \Delta_{max}$ with Δ_{max} being the maximum adjustable-delay.

III. DESIGN AND ANALYSIS OF RIS SPOOFING

In this section we focus on the design of the RIS for spoofing and analyze its impact on the sensing outcome.

A. Dynamic Phase Shifts Design

First, we can rewrite the matched-filtering output in (6) as:

$$C(\tau, \mu) = \left| \sqrt{P} \gamma_B \beta_V \mathbf{b}_B(\theta_V) \mathbf{a}_B^H(\theta_V) \mathbf{w} c_V(\tau, \mu) + \sqrt{P} \gamma_B \beta_R \mathbf{b}_B(\theta_R) \mathbf{a}_B^H(\theta_R) \mathbf{w} c_R(\tau, \mu) + \tilde{\mathbf{z}}_E(\tau, \mu) \right|^2, \quad (8)$$

where $c_V(\tau, \mu) \triangleq \int_0^T s(t - \tau_V) s^*(t - \tau) e^{-j2\pi(\mu - \mu_V)t} dt$, $c_R(\tau, \mu) \triangleq \int_0^T s(t - \tau_V) s^*(t - \tau) \left[\sum_{m=1}^M e^{-j(2\pi\mu t - \phi_m(t))} \right] dt$, and $\tilde{\mathbf{z}}_E(\tau, \mu) \triangleq \int_0^T \mathbf{z}_E(t) s^*(t - \tau) e^{-j2\pi\mu t} dt$. To spoof the sensing outcome, we assume that the RIS can derive $\Delta t_R = 2\frac{d_V - d_R}{c}$ by eavesdropping on the uplink communication of the VU [15]. Thus, $C(\tau, \mu)$ will only exhibit one peak around τ_V in the time domain. Moreover, we assume a perfect echo delay estimation $\hat{\tau}_V = \tau_V$ due to the high delay resolution in large bandwidth mmWave ISAC systems. In other words, we only focus on the spoofing on μ_V and θ_V .

Given (8), we can observe that the impact of RIS spoofing stems from the term $\sqrt{P} \gamma_B \beta_R \mathbf{b}_B(\theta_R) \mathbf{a}_B^H(\theta_R) \mathbf{w} c_R(\tau, \mu)$. Assuming $\hat{\tau}_V = \tau_V$, we have $c_V(\hat{\tau}_V, \mu) = \int_0^T e^{-j2\pi(\mu - \mu_V)t} dt$ and $c_R(\hat{\tau}_V, \mu) = \sum_{m=1}^M \int_0^T e^{-j(2\pi\mu t - \phi_m(t))} dt$. We can find that the peak position of $c_V(\hat{\tau}_V, \mu)$ in the frequency domain occurs at $\mu = \mu_V$. Thus, a natural analogy is to set $\phi_m(t) = 2\pi\mu_m t$ for artificially creating M peak positions at frequencies μ_1, \dots, μ_M . In practice, due to the hardware constraints of the RIS, the phase shift $\phi_m(t)$ on the m -th element can be only given in a discrete form as:

$$\phi_m(t) = (2\pi\mu_m \lceil \frac{t}{\Delta T} \rceil \Delta T) \bmod 2\pi, \quad (9)$$

where ΔT represents the shortest time interval over which $\phi_m(t)$ can vary. Meanwhile, the modulo operation is applied because the phase shifts of the RIS are typically confined to the range 0 to 2π . Given the design in (9), we focus on one fundamental spoofing case in which the M spoofing frequencies are set equal, i.e., $\mu_1 = \mu_2 = \dots = \mu_M = \tilde{\mu}$ such that $\hat{\mu}_V \triangleq \arg \max_{\mu} C(\hat{\tau}_V, \mu)$ is spoofed as $\tilde{\mu}$. To this end, the RIS should select $\tilde{\mu}$ such that the peak of $C(\hat{\tau}_V, \mu)$ occurs at $\tilde{\mu}$ rather than μ_V , i.e., $C(\hat{\tau}_V, \tilde{\mu}) \geq C(\hat{\tau}_V, \mu_V)$.

B. Impact on Doppler Shift Estimation

We begin by deriving the feasible spoofing frequency set $\mathcal{A} \triangleq \{\tilde{\mu} | C(\hat{\tau}_V, \tilde{\mu}) \geq C(\hat{\tau}_V, \mu_V)\}$. Since the matched-filtering output of noise is negligible compared to the spoofing echo, we can ignore $\tilde{\mathbf{z}}_E(\hat{\tau}_V, \mu)$ and rewrite $C(\hat{\tau}_V, \mu)$ as:

$$\begin{aligned} C(\hat{\tau}_V, \mu) &= \frac{P \gamma_B^2}{N_r} \sum_{n_r=1}^{N_r} \left| \beta_V g_{n_r}(\theta_0, \theta_V) c_V(\hat{\tau}_V, \mu) + \beta_R g_{n_r}(\theta_0, \theta_R) M c_R(\hat{\tau}_V, \mu) \right|^2 \\ &= \frac{PT^2 \gamma_B^2}{N_r} \sum_{n_r=1}^{N_r} \left| \beta_V g_{n_r}(\theta_0, \theta_V) e^{-j\pi(\mu - \mu_V)T} \text{sinc}(T(\mu - \mu_V)) + \beta_R g_{n_r}(\theta_0, \theta_R) M e^{j\pi\tilde{\mu}\Delta T} e^{-j\pi(\mu - \tilde{\mu})T} \text{sinc}(\mu\Delta T) \times f(K, \pi\Delta T(\mu - \tilde{\mu})) \right|^2, \end{aligned} \quad (10)$$

where we adopt a precoding vector $\mathbf{w} = \mathbf{a}_B(\theta_0)$ steered towards θ_0 , which may be selected from a pre-defined codebook [16]. Moreover, in (10), we define

$f(K, x) = \frac{\sin(Kx)}{K \sin x}$, $\text{sinc}(x) = \frac{\sin(\pi x)}{\pi x}$, and $g_{n_r}(\theta_1, \theta_2) = e^{-\frac{j\pi}{2}[\cos \theta_1(N_t-1) - \cos \theta_2(N_t+1-2n_r)]} f(N_t, \frac{\pi}{2}(\cos \theta_1 - \cos \theta_2))$. To derive the expression of \mathcal{A} , we first present the following lemma pertaining to a set of infeasible spoofing frequencies.

Lemma 1. *If the number of RIS reflecting elements satisfies $M \gg \sqrt{\frac{\kappa_V \lambda}{4\pi\eta S}} \left| \frac{f(N_t, \frac{\pi}{2}(\cos \theta_0 - \cos \theta_V))}{f(N_t, \frac{\pi}{2}(\cos \theta_0 - \cos \theta_R))} \right|$, an infeasible spoofing frequency set can be given by $\mathcal{A}_\emptyset = \{\mu \mid \mu = \mu_V + \frac{n}{\Delta T}, n \in \mathcal{Z}\}$, i.e., $\mathcal{A}_\emptyset \cap \mathcal{A} = \emptyset$.*

Proof. To prove Lemma 1, we can directly show that the inequality $C(\hat{\tau}_V, \mu_V) \geq C(\hat{\tau}_V, \tilde{\mu})$ holds for $\tilde{\mu} \in \mathcal{A}_\emptyset$ as follows:

$$\begin{aligned} & C(\hat{\tau}_V, \mu_V) \\ &= \frac{PT^2\gamma_B^2}{N_r} \sum_{n_r=1}^{N_r} \left| \beta_V g_{n_r}(\theta_0, \theta_V) + f(K, -\pi n) e^{j\pi \frac{n}{\Delta T} T} \times \right. \\ & \quad \left. M \beta_R g_{n_r}(\theta_0, \theta_R) e^{j\pi \mu_\emptyset \Delta T} \text{sinc}(\mu_V \Delta T) \right|^2 \\ & \stackrel{(a)}{\approx} \frac{PT^2\gamma_B^2}{N_r} \sum_{n_r=1}^{N_r} \left| M \beta_R g_{n_r}(\theta_0, \theta_R) e^{j\pi \mu_\emptyset \Delta T} \text{sinc}(\mu_V \Delta T) \right|^2 \\ & \stackrel{(b)}{>} \frac{PT^2\gamma_B^2}{N_r} \sum_{n_r=1}^{N_r} \left| M \beta_R g_{n_r}(\theta_0, \theta_R) e^{j\pi \mu_\emptyset \Delta T} \text{sinc}(\mu_V \Delta T + n) \right|^2 \\ & = C(\hat{\tau}_V, \mu_\emptyset). \end{aligned} \quad (11)$$

Approximation (a) holds for $\forall n_r \in \{1, \dots, N_r\}$, when $|f(K, -\pi n) e^{j\pi \frac{n}{\Delta T} T} M \beta_R g_{n_r}(\theta_0, \theta_R) e^{j\pi \mu_\emptyset \Delta T} \text{sinc}(\mu_V \Delta T)| \gg |\beta_V g_{n_r}(\theta_0, \theta_V)|$, which is equivalent to the condition $M \gg \sqrt{\frac{\kappa_V \lambda}{4\pi\eta S}} \left| \frac{f(N_t, \frac{\pi}{2}(\cos \theta_0 - \cos \theta_V))}{f(N_t, \frac{\pi}{2}(\cos \theta_0 - \cos \theta_R))} \right|$. Inequality (b) holds because $|\text{sinc}(\mu_V \Delta T)| > |\text{sinc}(\mu_V \Delta T + n)|, \forall n \in \mathcal{Z}$. \square

Given Lemma 1, if we only consider $\tilde{\mu} \in \mathcal{A}$, i.e., $\tilde{\mu} \notin \mathcal{A}_\emptyset$, $C(\hat{\tau}_V, \mu)$ in (10) can be approximated by:

$$\begin{aligned} C(\hat{\tau}_V, \mu) \approx & PT^2\gamma_B^2 \left[C_V \text{sinc}^2(T(\mu - \mu_V)) + \right. \\ & \left. M^2 C_R \text{sinc}^2(\mu \Delta T) f^2(K, \pi \Delta T(\mu - \tilde{\mu})) \right], \end{aligned} \quad (12)$$

where the cross-product terms in the quadratic expansion are ignored since $f(K, \pi \Delta T(\mu - \tilde{\mu})) \text{sinc}(T(\mu - \mu_V)) \approx 0$ when $\tilde{\mu} \notin \mathcal{A}_\emptyset$. In (12), we further define $C_V \triangleq \beta_V^2 f^2(N_t, \frac{\pi}{2}(\cos \theta_0 - \cos \theta_V))$ and $C_R \triangleq \beta_R^2 f^2(N_t, \frac{\pi}{2}(\cos \theta_0 - \cos \theta_R))$. Another observation in (12) is that the impact of the spoofing frequency $\tilde{\mu}$ is periodic, as shown in the periodic spoofing term $M^2 C_R \text{sinc}^2(\mu \Delta T) f^2(K, \pi \Delta T(\mu - \tilde{\mu}))$. Specifically, the spoofing frequency $\tilde{\mu}$ will lead to multiple peaks at $\mu = \tilde{\mu} + \frac{n}{\Delta T}, n \in \mathcal{Z}$. Therefore, in order to derive \mathcal{A} , we only consider the highest peak defined in Lemma 2.

Lemma 2. *If the condition on M in Lemma 1 is satisfied, the highest peak of the spoofing term in (12) will be given by $\Delta \tilde{\mu} \triangleq \tilde{\mu} \bmod \frac{1}{\Delta T}$.*

Proof. Since the periodic function $f^2(K, \pi \Delta T(\mu - \tilde{\mu}))$ has sharp peaks at $\mu = \tilde{\mu} + \frac{n}{\Delta T}, n \in \mathcal{Z}$, the product $\text{sinc}^2(\mu \Delta T) f^2(K, \pi \Delta T(\mu - \tilde{\mu}))$ will also have peaks at these frequencies. Moreover, the highest peak among $\mu = \tilde{\mu} + \frac{n}{\Delta T}, n \in \mathcal{Z}$ depends on the magnitude of $\text{sinc}^2(\mu \Delta T)$. Given $\mu = \tilde{\mu} + \frac{n}{\Delta T}, n \in \mathcal{Z}$, we further observe that $\text{sinc}^2(\mu \Delta T) = \text{sinc}^2(\tilde{\mu} \Delta T + n)$. Thus, we can find that the highest magnitude of $\text{sinc}^2(\mu \Delta T)$ locates at $\Delta \tilde{\mu} \triangleq \tilde{\mu} \bmod \frac{1}{\Delta T}$, i.e., the positive frequency closest to 0. \square

Given the result in Lemma 2, the possible spoofing frequency is restricted in $(0, \frac{1}{\Delta T}]$. In other words, an RIS capable changing its phase shift more frequently, i.e., operating with a smaller ΔT , will have a broader range of spoofing frequencies $\Delta \tilde{\mu}$. Moreover, the feasible spoofing frequency set should be redefined as $\mathcal{A} \triangleq \{\Delta \tilde{\mu} \mid C(\hat{\tau}_V, \Delta \tilde{\mu}) \geq C(\hat{\tau}_V, \mu_V)\}$, which is derived next.

Theorem 1. *Under the condition on M in Lemma 1, the feasible spoofing frequency set is given in (13).*

Proof. The proof can be directly completed by finding $\Delta \tilde{\mu}$ that satisfies $C(\hat{\tau}_V, \Delta \tilde{\mu}) \geq C(\hat{\tau}_V, \mu_V)$ based on (12). \square

Theorem 1 indicates that, if the RIS selects a spoofing frequency $\Delta \tilde{\mu} \in \mathcal{A}$, the estimated Doppler shift will be spoofed as $\hat{\mu}_V = \Delta \tilde{\mu}$. According to the derived result in (13), the range of feasible spoofing frequencies expands as more reflecting elements are deployed at the RIS. In addition, the beam orientation θ_0 also influences the set \mathcal{A} . Generally, when θ_0 is closer to the VU's AoD θ_V , the spoofing set \mathcal{A} becomes narrower, whereas a beam direction closer to the RIS's AoD θ_R leads to a wider set. This phenomenon poses a critical challenge when ISAC is leveraged for beam tracking. For instance, when a VU moves through the coverage of the RSU, there inevitably exists moments when the beam is steered closer to the RIS. At such instances, the RIS can select a spoofing frequency $\Delta \tilde{\mu}$ that results significant beam misalignment in the subsequent tracking step. More critically, this misalignment may accumulate over time, leading the RSU to lose track of the VU eventually.

C. Impact on AoD MLE

Given the estimated $\hat{\tau}_V$ and $\hat{\mu}_V$, the RSU will continue to estimate θ_V . First, the compensated and normalized echo is given by:

$$\hat{\mathbf{y}}_E \triangleq \frac{1}{\sqrt{P}\gamma_B} \int_0^T \mathbf{y}_E(t) s^*(t - \hat{\tau}) e^{-j2\pi \Delta \tilde{\mu} t} dt. \quad (14)$$

We next define a perfect MLE $\tilde{\theta}_V$ obtained without spoofing and examine the deviation between the spoofed MLE $\hat{\theta}_V$ and $\tilde{\theta}_V$. First, we rewrite (14) as:

$$\begin{aligned} \hat{\mathbf{y}}_E = & T \beta_V \mathbf{b}_B(\theta_V) h(\theta_V, \theta_0) e^{-j\pi(\Delta \tilde{\mu} - \mu_V)T} \text{sinc}(T(\Delta \tilde{\mu} - \mu_V)) \\ & + MT \beta_R \mathbf{b}_B(\theta_R) h(\theta_R, \theta_0) e^{j\pi \Delta \tilde{\mu} \Delta T} \text{sinc}(\Delta \tilde{\mu} \Delta T) + \hat{\mathbf{z}}_E, \end{aligned} \quad (15)$$

$$\mathcal{A} = \{ \Delta\tilde{\mu} \mid M^2 C_R [\text{sinc}^2(\Delta\tilde{\mu}\Delta T) - \text{sinc}^2(\mu_V\Delta T)f^2(K, \pi\Delta T(\mu_V - \Delta\tilde{\mu}))] - C_V [1 - \text{sinc}^2(T(\mu_V - \Delta\tilde{\mu}))] \geq 0 \}. \quad (13)$$

where $\hat{\mathbf{z}}_E = \frac{\hat{\mathbf{z}}_E(\hat{\tau}, \Delta\tilde{\mu})}{\sqrt{P}\gamma_B} \sim \mathcal{CN}(\mathbf{0}_{N_r}, \frac{\sigma^2 T}{P\gamma_B^2} \mathbf{I}_{N_r})$ and $h(\theta_1, \theta_2) = e^{-\frac{j\pi(N_t-1)}{2}[\cos\theta_1 - \cos\theta_2]} f(N_t, \frac{\pi}{2}(\cos\theta_1 - \cos\theta_2))$. Similar to (7), we define the perfect MLE without spoofing as follows:

$$\hat{\theta}_V = \arg \max_{\theta_V} p(\hat{\mathbf{y}} \mid \theta_V), \quad (16)$$

where $\hat{\mathbf{y}} = T\beta_V \mathbf{b}_B(\theta_V)h(\theta_V, \theta_0) + \hat{\mathbf{z}}_E$. Here, $\hat{\mathbf{y}}$ represents the normalized received signal compensated by perfect estimation $\hat{\tau}_V = \tau_V$ and $\hat{\mu}_V = \mu_V$, without the RIS spoof. Thus, $\hat{\theta}_V$ in (16) is the best MLE on θ_V we can obtain.

Next, we derive the deviation between the perfect MLE $\hat{\theta}_V$ and the spoofed MLE $\tilde{\theta}_V$ in the following theorem.

Theorem 2. Assume the perfect delay estimation $\hat{\tau}_V = \tau_V$ and spoofed Doppler shift estimation $\hat{\mu}_V = \Delta\tilde{\mu}$ are obtained under RIS spoofing. The spoofed MLE $\tilde{\theta}_V$ can be given by:

$$\hat{\theta}_V = \arg \min_{\theta_V} \left[\|\hat{\mathbf{y}} - T\beta_V \mathbf{b}_B(\theta_V)h(\theta_V, \theta_0)\|^2 + 2T\beta_V \sum_{n=1}^{N_r} \Re\{\Delta\hat{y}_n g_n^*(\theta_V, \theta_0)\} \right], \quad (17)$$

where $\Delta\hat{\mathbf{y}} \triangleq \hat{\mathbf{y}}_E - \hat{\mathbf{y}} = [\Delta\hat{y}_1, \dots, \Delta\hat{y}_{N_r}]^T$. Moreover, the perfect MLE $\hat{\theta}_V$ defined in (16) can be similarly given by:

$$\tilde{\theta}_V = \arg \min_{\theta_V} \|\hat{\mathbf{y}} - T\beta_V \mathbf{b}_B(\theta_V)h(\theta_V, \theta_0)\|^2. \quad (18)$$

Proof. We first derive $\tilde{\theta}_V$ defined in (16). Since $\hat{\mathbf{y}} = T\beta_V \mathbf{b}_B(\theta_V)h(\theta_V, \theta_0) + \hat{\mathbf{z}}_E$ and $\hat{\mathbf{z}}_E \sim \mathcal{CN}(\mathbf{0}_{N_r}, \frac{\sigma^2 T}{P\gamma_B^2} \mathbf{I}_{N_r})$, (18) can be directly obtained based on the probability distribution function (PDF) of multivariate normal distribution. For the spoofed MLE, since the RSU is unaware of the presence of the malicious RIS, $\tilde{\theta}_V$ is obtained by directly replacing $\hat{\mathbf{y}}$ in (18) with the superimposed echo $\hat{\mathbf{y}}_E$ as:

$$\hat{\theta}_V = \arg \min_{\theta_V} \|\hat{\mathbf{y}}_E - T\beta_V \mathbf{b}_B(\theta_V)h(\theta_V, \theta_0)\|^2. \quad (19)$$

We can further derive (19) as following

$$\begin{aligned} \hat{\theta}_V &= \arg \min_{\theta_V} \|\hat{\mathbf{y}}_E - \hat{\mathbf{y}} + \hat{\mathbf{y}} - T\beta_V \mathbf{b}_B(\theta_V)h(\theta_V, \theta_0)\|^2 \\ &= \arg \min_{\theta_V} \|\hat{\mathbf{y}} - T\beta_V \mathbf{b}_B(\theta_V)h(\theta_V, \theta_0)\|^2 - \\ &\quad 2\Re\{(\hat{\mathbf{y}}_E - \hat{\mathbf{y}})^H (\hat{\mathbf{y}} - T\beta_V \mathbf{b}_B(\theta_V)h(\theta_V, \theta_0))\} \\ &= \arg \min_{\theta_V} \left[\|\hat{\mathbf{y}} - T\beta_V \mathbf{b}_B(\theta_V)h(\theta_V, \theta_0)\|^2 + \right. \\ &\quad \left. 2T\beta_V \sum_{n=1}^{N_r} \Re\{\Delta\hat{y}_n g_n^*(\theta_V, \theta_0)\} \right], \end{aligned} \quad (20)$$

which completes the proof. \square

From Theorem 2, we can observe that the spoofed MLE deviates from the perfect MLE because of the term $2T\beta_V \sum_{n=1}^{N_r} \Re\{\Delta\hat{y}_n g_n^*(\theta_V, \theta_0)\}$, which is introduced by the

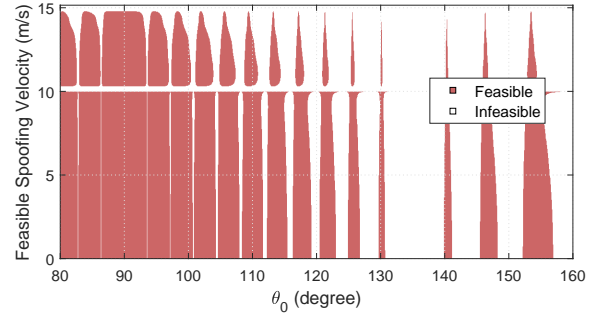


Fig. 3. Feasible spoofing velocity versus beam steering direction.

malicious RIS. Although it is challenging to derive a closed-form expression for $|\tilde{\theta}_V - \hat{\theta}_V|$, we can still find that a spoofed MLE $\tilde{\theta}_V \neq \hat{\theta}_V$ will be obtained if the minimum of $\|\hat{\mathbf{y}} - T\beta_V \mathbf{b}_B(\theta_V)h(\theta_V, \theta_0)\|^2$ shifts after adding the term $2T\beta_V \sum_{n=1}^{N_r} \Re\{\Delta\hat{y}_n g_n^*(\theta_V, \theta_0)\}$.

IV. SIMULATION RESULTS AND ANALYSIS

For our simulations, we consider a two dimensional Cartesian coordinate system with the RSU located at its origin. The AoDs of the VU and RIS are $\theta_V = 135^\circ$ and $\theta_R = 90^\circ$. The coordinates of the VU and RIS are $(x_V, y_V) = (40 \times \cos\theta_V, 40 \times \sin\theta_V)$ and $(x_R, y_R) = (30 \times \cos\theta_R, 30 \times \sin\theta_R)$ both in meters. The other parameters are set as follows unless specified otherwise later: $P = 30$ dBm, $\sigma^2 = -130$ dBm, $f_c = 28$ GHz, $N_t = N_r = 32$, $M = 32$, $\kappa_V = 7$ dBsm, $\eta = 0.8$, $S = 50$ cm \times 10 cm, $T = 10$ ms, and $\Delta T = 1$ ms. The VU is assumed to move along the positive x-axis at a speed of $v = 10$ m/s, and, thus, the Doppler shift can be derived as $\mu_V = v f_c \cos(\pi - \theta_V)$.

Fig. 3 shows the impact of RIS spoofing on the estimated velocity of the VU, which can be derived by the spoofed Doppler shift. In particular, the different feasible spoofing velocity sets, derived from (13), versus RSU's beam steering direction θ_0 are illustrated. From Fig. 3, we can observe that, generally, a beam steered closer to VU's AoD $\theta_V = 135^\circ$ can eliminate the impact of RIS spoofing. For instance, when $\theta_0 \in (131^\circ, 140^\circ)$, we have $\mathcal{A} = \emptyset$, indicating that no successful spoofing can be conducted. However, as θ_0 is in the vicinity of $\theta_R = 90^\circ$, i.e., steered towards the RIS, the RSU may obtain a spoofed velocity ranging from 0.1 m/s to 14.9 m/s, introducing a significant deviation of -9.9 m/s to 4.9 m/s with respect to the true value $v = 10$ m/s.

Fig. 4 shows the range of feasible spoofing velocity, i.e., the difference between maximal and minimal spoofing velocities, versus the number of RIS reflecting elements. We can see that the range of feasible spoofing velocity expands as the number of reflecting elements increases, except when the RSU's beam is set to be perfectly steered towards the VU with $\theta_0 = 135^\circ$. Moreover, we can observe that the range is large for $\theta_0 = 90^\circ$

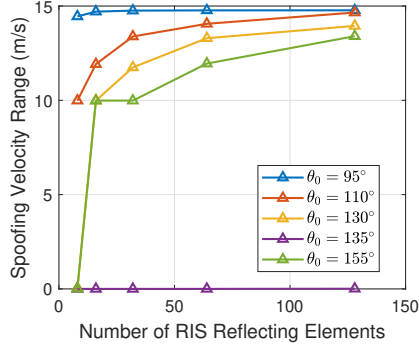


Fig. 4. Spoofing velocity range versus number of RIS reflecting elements.

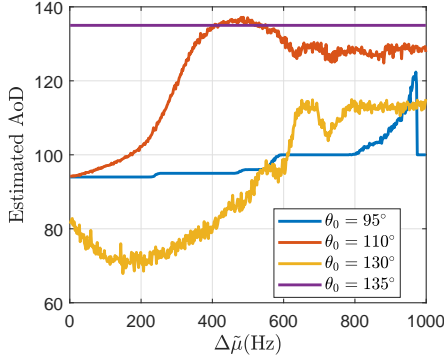


Fig. 5. Impact of Doppler shift spoofing on the resulted MLE of AoD.

and $\theta_0 = 110^\circ$ since these θ_0 are close to the RIS. However, the range is only 1 m/s lower for $\theta_0 = 130^\circ$ with only 5° misalignment with respect to θ_V . Moreover, even if the beam direction is far to both VU and RIS, the spoofing can be still conducted as long as the RIS is equipped with enough reflecting elements, as shown in the case $\theta_0 = 155^\circ$.

In Fig. 5, we show the spoofed MLE for AoD as a function of the spoofing frequency on the Doppler shift estimation. The estimated AoD are averaged over 2,000 trials of independent noise. First, we can observe that the MLE for AoD will not be affected under a beam perfectly steered to the VU when $\theta_0 = 135^\circ$. However, the RIS can always find a spoofing frequency that causes a severe deviation of the spoofed MLE under beam misalignment. For instance, when $\theta_0 = 130^\circ$ is only 5° deviating from θ_V , its MLE can be spoofed as 70° with $\Delta\tilde{\mu} = 180$ Hz, which leads to an estimation error of 65° .

V. CONCLUSION

In this paper, we have investigated a novel RIS-aided spoofing strategy that compromises the sensing safety of the ISAC system. In particular, we have proposed a time-varying phase shift design at the RIS to spoof the RSU's sensing outcome of the VU's Doppler shift and AoD. Moreover, we have analytically derived the feasible spoofing frequency set with respect to the Doppler shift and the deviation of the

spoofed MLE for AoD. The derived expression has indicated that the number of reflecting elements at the RIS and its AoD with respect to the RSU significantly affect the spoofed sensing outcome. Simulation results demonstrate that, even with a beam misalignment of only 5° with respect to the VU, the RIS-aided spoofing can lead to a relative velocity estimation error ranging from -9.9 m/s to 4 m/s and an AoD estimation error of up to 65° .

REFERENCES

- [1] Z. Wei, F. Liu, C. Masouros, N. Su, and A. P. Petropulu, "Toward Multi-Functional 6G Wireless Networks: Integrating Sensing, Communication, and Security," *IEEE Communications Magazine*, vol. 60, no. 4, pp. 65–71, 2022.
- [2] N. Su, F. Liu, and C. Masouros, "Secure Radar-Communication Systems With Malicious Targets: Integrating Radar, Communications and Jamming Functionalities," *IEEE Transactions on Wireless Communications*, vol. 20, no. 1, pp. 83–95, 2021.
- [3] N. Su, F. Liu, Z. Wei, Y.-F. Liu, and C. Masouros, "Secure Dual-Functional Radar-Communication Transmission: Exploiting Interference for Resilience Against Target Eavesdropping," *IEEE Transactions on Wireless Communications*, vol. 21, no. 9, pp. 7238–7252, 2022.
- [4] N. Su, F. Liu, and C. Masouros, "Sensing-Assisted Eavesdropper Estimation: An ISAC Breakthrough in Physical Layer Security," *IEEE Transactions on Wireless Communications*, vol. 23, no. 4, pp. 3162–3174, 2024.
- [5] Y. Cao, L. Duan, and R. Zhang, "Sensing for Secure Communication in ISAC: Protocol Design and Beamforming Optimization," *IEEE Transactions on Wireless Communications*, vol. 24, no. 2, pp. 1207–1220, 2025.
- [6] B. Zheng, X. Xiong, T. Ma, J. Tang, D. W. K. Ng, A. L. Swindlehurst, and R. Zhang, "Intelligent Reflecting Surface-Enabled Anti-Detection for Secure Sensing and Communications," *IEEE Wireless Communications*, vol. 32, no. 2, pp. 156–163, 2025.
- [7] F. Xu, W. Lai, and K. Shen, "Intelligent Surface Assisted Radar Stealth Against Unauthorized ISAC," *IEEE Wireless Communications Letters*, vol. 14, no. 4, pp. 1149–1153, 2025.
- [8] X. Shao and R. Zhang, "Target-Mounted Intelligent Reflecting Surface for Secure Wireless Sensing," *IEEE Transactions on Wireless Communications*, vol. 23, no. 8, pp. 9745–9758, 2024.
- [9] B. Zheng, X. Xiong, J. Tang, and R. Zhang, "Intelligent Reflecting Surface-Aided Electromagnetic Stealth Against Radar Detection," *IEEE Transactions on Signal Processing*, vol. 72, pp. 3438–3452, 2024.
- [10] H. Wang, B. Zheng, X. Shao, and R. Zhang, "Intelligent Reflecting Surface-Aided Radar Spoofing," *IEEE Wireless Communications Letters*, vol. 13, no. 10, pp. 2722–2726, 2024.
- [11] F. Liu, W. Yuan, C. Masouros, and J. Yuan, "Radar-Assisted Predictive Beamforming for Vehicular Links: Communication Served by Sensing," *IEEE Transactions on Wireless Communications*, vol. 19, no. 11, pp. 7704–7719, 2020.
- [12] G. C. Trichopoulos, P. Theofanopoulos, B. Kashyap, A. Shekawat, A. Modi, T. Osman, S. Kumar, A. Sengar, A. Chang, and A. Alkhatieb, "Design and Evaluation of Reconfigurable Intelligent Surfaces in Real-World Environment," *IEEE Open Journal of the Communications Society*, vol. 3, pp. 462–474, 2022.
- [13] Z. Du, F. Liu, W. Yuan, C. Masouros, Z. Zhang, S. Xia, and G. Caire, "Integrated Sensing and Communications for V2I Networks: Dynamic Predictive Beamforming for Extended Vehicle Targets," *IEEE Transactions on Wireless Communications*, vol. 22, no. 6, pp. 3612–3627, 2023.
- [14] J. An, C. Xu, D. W. K. Ng, C. Yuen, and L. Hanzo, "Adjustable-Delay RIS Is Capable of Improving OFDM Systems," *IEEE Transactions on Vehicular Technology*, vol. 73, no. 7, pp. 9927–9942, 2024.
- [15] X. Shao, C. You, W. Ma, X. Chen, and R. Zhang, "Target Sensing With Intelligent Reflecting Surface: Architecture and Performance," *IEEE Journal on Selected Areas in Communications*, vol. 40, no. 7, pp. 2070–2084, 2022.
- [16] R. Li, X. Shao, S. Sun, M. Tao, and R. Zhang, "IRS Aided Millimeter-Wave Sensing and Communication: Beam Scanning, Beam Splitting, and Performance Analysis," *IEEE Transactions on Wireless Communications*, vol. 23, no. 12, pp. 19 713–19 727, 2024.